Environmental Science Processes & Impacts

PAPER

View Article Online
View Journal

Cite this: DOI: 10.1039/d5em00654f

Organic composition of ultrafine particles formed from automotive braking

A. E. Thomas, V. Perraud, M. Lee, B. Rojas, M. E. Cooke, L. M. Wingen, P. S. Bauer, M. Dam, B. J. Finlayson-Pitts and J. N. Smith *

Non-exhaust emissions (*e.g.*, automotive brake and tire wear) are quickly replacing exhaust emissions as the dominant traffic particulate pollutant. A significant fraction of the emissions are complex mixtures of organic compounds whose composition is not well known. Due to their unique health implications, knowledge of the composition of ultrafine particles (<100 nm in diameter) is of particular interest. Here we report on the size-selected organic composition of ultrafine particles nucleated during high brake temperature conditions generated using a custom brake dynamometer system and two common brake pad types. Using high resolution mass spectrometry, we find that the organic composition of these particles is dominated by species containing oxygen (CHO) and nitrogen (CHN/CHON). Many of these compounds are unsaturated and are attributed to the thermal degradation of resin material used in the pad formulation. Other abundant compounds include various glycols and amines, several of which are unequivocally identified and discussed as potential marker compounds for brake wear emissions. A significant fraction of highly oxidized, low volatility species observed in ultrafine particles could not be conclusively attributed to the thermal degradation of the brake material, indicating the presence of chemical pathways unique to the frictional heating process. This emphasizes the importance of using a brake dynamometer to generate brake wear particles as opposed to other strategies.

Received 20th August 2025
Accepted 16th October 2025

DOI: 10.1039/d5em00654f

rsc.li/espi

Environmental significance

The air pollution burden from motor vehicles has been substantially reduced over the last decades due to the ongoing global transition to alternative fuels and vehicle electrification. Emissions from brake wear and other non-exhaust sources are therefore expected to be the predominant traffic pollutants in the future. The environmental impacts of different brake wear emissions including particles are uncertain due to significant knowledge gaps about their chemical composition. We show that ultrafine particles formed from automotive braking are comprised of a complex array of organic molecules, many of which absorb light at wavelengths that can directly impact climate. Species identified in this study can potentially be used to better quantify real-world brake wear particle emissions in the future.

1 Introduction

Road traffic is a significant contributor to urban air pollution, serving as a major source of nitrogen oxides (NO_x), volatile organic compounds (VOCs), and particulate matter (PM).[1–4] These emissions negatively impact human health[5,6] and disproportionally affect communities that live near major roadways, including economically disadvantaged communities and communities of color.[7–10] While the past decades have seen dramatic reductions in the air pollutant contributions from vehicular exhaust in response to regulatory efforts,[11–13] emissions from non-exhaust sources such as brake and tire wear[14–16] persist and are currently unfettered by emission control legislation in many regions. Automotive brake wear serves as a non-exhaust emission source of particular relevance, having been estimated to contribute up to roughly half of the PM mass from non-exhaust sources[17] and up to 21% of traffic-related PM.[18,19] In addition, brake wear has recently been shown to emit a wide variety of gas-phase species,[20–23] many of which are atmospherically reactive and undergo secondary chemistry in air to form other air pollutants including particles,[24] though the magnitude of this contribution remains largely unknown.

As vehicle electrification and the transition to alternative fuels progresses,[25] brake wear and other non-exhaust emission sources are quickly emerging as the predominant traffic PM pollutants in the atmosphere.[14–16] To fully ascertain the implications for air quality, human health, and climate, a thorough understanding of the physicochemical properties of brake wear emissions is needed. While evidence already exists that inhalation of brake wear particles (BWPs) can induce DNA damage, oxidative stress, and pulmonary inflammation in mammalian models,[26–31] the mechanism by which this occurs remains poorly understood, but is suspected to be related to their

Department of Chemistry, University of California, Irvine, USA. E-mail: jimsmith@uci.edu

composition.[32] Fang *et al.*[27] observed that BWPs generated OH radicals in aqueous solution, potentially explaining some of the health effects such as oxidative stress. The authors hypothesized that this production was due to aqueous chemistry of organic components in the brake pad because of modest correlations between OH and BWP organic/elemental carbon mass concentrations. The metal composition of BWPs has been reported rather extensively,[4,33–35] but fewer reports exist on organic speciation. Alves *et al.*[36] identified more than 150 organic compounds in brake wear PM_{10} with gas chromatography-mass spectrometry, revealing a complex mixture of species present in BWPs including aliphatic, aromatic, glycolic, and phenolic constituents. The authors noted substantial variability in compound distributions depending on brake pad type tested.

BWPs can be emitted from both primary and secondary formation pathways. Primary BWPs are formed directly from the abrasive contact between brake pad and rotor, resulting in the generation of particles with diameters mostly above 200 nm,[37,38] though the particle sizes observed depend greatly on the testing method and braking cycle. Frictional heating under high braking force conditions results in the secondary formation or nucleation of BWPs, where emitted gases condense to form new particles. BWP nucleation is reported to occur above a certain critical brake temperature (hereafter referred as T_{crit}) reportedly ranging between 70 °C for railway brakes up to 475 °C for automobile brakes.[39–42] Most automotive brake pads consist of five common components:[43,44] friction material, binders (most commonly phenolic resin),[45,46] fillers (which can include tire rubber),[47] lubricants, and reinforcement fibers, although the exact materials and component ratios mixed could vary substantially with the particular manufacturer formulation and vehicle type, presumably contributing to the observed variability in T_{crit}. While the extent to which BWP nucleation occurs in real environments is unclear, there is nevertheless significant overlap between the reported range of T_{crit} values and rotor temperatures achieved for common passenger vehicles,[48] suggesting BWP nucleation may be contributing to traffic-related particle number concentrations in urban environments. Crucial to efforts to quantify the impacts of different brake wear emission pathways is the identification of unique chemical markers in controlled, laboratory-generated emissions. Although certain metals such as antimony and barium have been proposed as markers,[49,50] they may not be unique nor capture processes such as nucleation from organic vapors.

The occurrence of BWP nucleation is marked by the appearance of high concentrations of ultrafine (<100 nm in diameter) particles (hereafter referred to as UBWPs).[39–42] Ultrafine particles have unique properties, including the ability to enter the bloodstream and cross the blood–brain barrier after inhalation, causing a wide array of adverse health effects.[51–54] In addition, ultrafine particles impact visibility and climate by serving as a globally significant source of seeds for haze and cloud droplet formation, or cloud condensation nuclei.[55,56] Key to discerning ultrafine particle health effects as well as impacts on climate and visibility is an understanding of their chemical composition. Given the large quantities of reactive VOCs emitted during harsh braking,[22] it is reasonable to suspect that UBWPs are formed from the condensation of gases emitted upon the thermal desorption and/or degradation of organic components in the brake pad such as phenolic resin.

Here we characterize the organic composition of UBWPs generated from two common brake pad types (ceramic and semi-metallic) using a custom-built brake dynamometer. To investigate the sources of the observed compounds, observations from additional experiments are also presented including the organic composition of particles nucleated from the direct heating of the brake pads and a commercial phenolic resin. Due to its suspected role in UBWP nucleation, a more detailed analysis of emissions from phenolic resin thermal degradation including gas and particle phase organic speciation will be included in a future manuscript. The organic composition of the brake pads themselves is also reported here. Some of the most abundant compounds observed from the different datasets are unequivocally identified and their potential to serve as BWP markers is discussed.

2 Materials and methods

2.1 Brake dynamometer experiments

Fig. S1 shows a schematic of the brake dynamometer experiment layout. A custom-built brake dynamometer was used to generate brake wear particles that has been described in detail elsewhere,[22,57] with important details provided in the SI.

Two common brake formulations were tested: a ceramic brake pad (Kodiak, model DBC-225), also sometimes referred to as a non-asbestos organic brake pad, and a semi-metallic brake pad (BrakeBest, model MKD289). For each experiment, a cycle of 8 s light braking pulses (~15–20 psi brake pressure, ~100–150 N m brake torque) spaced in between 45 s cruising times (no braking) was first administered for 30 min, followed by a cycle of 10 s harsher braking pulses (~25 psi, ~200 N m) spaced in between 30 s cruising times to initiate UBWP nucleation. The two braking cycles were implemented to probe different temperature and braking torque scenarios such as those observed in urban street (light braking) *versus* highway (harsh braking) environments.[58] Similar to previous work using this dynamometer,[22,57] each brake pad used in the present study underwent several braking cycles as described above, reaching rotor temperatures >200 °C, to better represent the composition of brake wear particles that may be generated during the bulk lifetime of a brake pad fitted to an automotive vehicle.

Particle number-size distributions were collected across a broad diameter range (4 nm–22 μm) to comprehensively monitor BWP formation characteristics before and during each nucleation event. Two scanning mobility particle sizer (SMPS) systems were employed, one consisting of a nano-differential mobility analyzer (TSI, model 3085) scanning mobility diameters 4–40 nm paired with an ultrafine condensation particle counter (TSI, model 3776), and a second consisting of long differential mobility analyzer (TSI, model 3081) scanning diameters 12–730 nm paired with a mixing condensation particle counter (Brechtel Manufacturing, Inc., model 1720). An aerodynamic particle sizer (APS; TSI, model 3321) measured particles of aerodynamic diameters 0.544–22 μm.

2.2 Thermal degradation experiments

A series of supporting experiments were conducted using a different apparatus (Fig. S2A) to probe the composition of particles nucleated from the thermal degradation of a commercial phenolic resin powder (part 135-10005, Allied High Tech Productions, Inc.) as well as the automotive brake pads tested in the dynamometer experiments. Although evaporation and thermal degradation of organics could both be occurring during heating, for simplicity these experiments are hereafter referred to as "thermal degradation" experiments. Phenolic resin is a major component of many automotive brake pad formulations, where it is used as a binder to hold other friction materials (*e.g.*, metals) together.[44] Comparison of the composition of particles from the thermal degradation of the resin to that of the UBWPs generated in the brake dynamometer was carried out to help identify sources of the observed organics. Phenolic resin is a synthetic polymer formed by reacting phenol with formaldehyde. The polymer is typically set to form a solid material by reacting with hexamethylenetetramine (HMTA, $C_6H_{12}N_4$) at high temperatures, forming cross-linking bonds that impart thermal stability to the polymer in a process known as curing.[59,60] Commercial resins typically contain HMTA and other additives in addition to the cross-linked polymer itself. As different automotive brake pads can contain phenolic resin binders of various stages of curing,[61] particle nucleation from thermal degradation at a variety of temperatures was studied.

Phenolic resin (2.5 g) was placed into a prebaked (to 350 °C) aluminum foil boat (Fig. S2B) and housed in a prebaked, ~100 mL stainless steel chamber. A gas chromatography oven was used to subject the resin to a controlled heat ramp from room temperature to 125 °C, 200 °C, and 250 °C. After cooling to room temperature, the resin then underwent a subsequent ramp to 300 °C to observe the organics desorbed from a highly cured resin material. Clean air was provided at 5 L min^{-1} to the chamber by a zero air generator (Aadco Instruments, model 747-30).

To isolate the organics in UBWPs that could be attributed to thermal degradation of the brake pad material itself (as opposed to abrasion or other frictional processes), the same apparatus was used to thermally degrade samples of both brake pad linings tested in the dynamometer experiments (Fig. S2B and C). New brake lining material (17.7 g of semi-metallic pad and 15.2 g of ceramic pad) that had been mechanically broken into pieces ~5–15 mm in diameter was subjected to a similar heat ramp as described above but with a maximum temperature of 250 °C, reflecting the upper range of T_{crit} values observed in our dynamometer experiments (Table S1). A purge gas generator (Parker-Balston, model 75-62) flowing at 12 L min^{-1} provided clean air for the brake pad thermal degradation experiments.

2.3 Thermal desorption chemical ionization mass spectrometry (TDCIMS) analysis

Ultrafine particle composition was characterized in real-time by thermal desorption chemical ionization mass spectrometry (TDCIMS). TDCIMS is an instrument designed to probe the size-resolved chemical composition of ultrafine particles.[62,63] Briefly, particles were charged using a unipolar charger and ultrafine modes were size-selected using a radial differential mobility analyzer (RDMA).[64] Ultrafine particles were collected *via* electrostatic deposition onto a platinum (Pt) filament biased at 3.5 kV, which was then moved to an ion source region. The filament was resistively heated in a 70 s ramp to 600 °C to thermally desorb the molecular constituents of the particles. These in turn underwent chemical ionization by reacting with either $(H_2O)_nH_3O^+$ or $(H_2O)_nO_2^-$ ($n = 1$–3) reagent ions for detection in the positive and negative ion modes, respectively. Reagent ions were obtained by passing 0.9 L min^{-1} of nitrogen (N_2) from the headspace of a liquid nitrogen dewar over nanopure water (18.2 MOhm cm; Barnstead, Thermo Scientific) contained in a glass trap and then exposing the airstream to a ^{210}Po radioactive source. Analyte ions are analyzed with a high-resolution time-of-flight mass spectrometer (Tofwerk AG, HTOF mass analyzer).

For the dynamometer experiments, particles with an electrical mobility diameter of 30 nm were selected, while the Pt filament was set to collect for 3 min and 5 min for positive and negative ion modes, respectively. In the phenolic resin thermal degradation experiments, where particles were formed by nucleation, the TDCIMS operated in "bulk" sampling mode, meaning sampled aerosols bypassed the RDMA and were directly deposited onto the filament for 1–2 min after charging. For all experiments, the sample inlet flow was 3.2 L min^{-1}, and background measurements were obtained immediately following particle collections by sampling chamber air without a voltage applied to the Pt filament, preventing electrostatic deposition. Data were processed using Tofware[65] (Aerodyne Research Inc., version 4.0) and a program developed in-house for additional processing such as background and baseline signal subtractions.

2.4 Liquid chromatography-mass spectrometry (LC-MS) analysis

Particles were also collected for offline organic composition analysis. From the dynamometer, UBWPs were collected during harsh braking cycles onto 47 mm diameter, 0.5 μm pore size PTFE filters (SKC West Inc.) after first passing through a Micro-orifice Uniform Deposit Impactor (MOUDI, MSP Corporation, model 100) equipped with two stages with calibrated cutoff sizes of 1000 nm and 89 nm,[66] preventing particles above an aerodynamic diameter of 89 nm from impacting onto the downstream filter. Dynamometer air was sampled at a flow rate of 6 L min^{-1} and mixed with 24 L min^{-1} of clean air from a purge gas generator (Parker-Balston, model 75-62) to achieve the required MOUDI inlet flow of 30 L min^{-1}. MOUDI sampling stages were covered with a thin layer of high vacuum silicone grease (Dow Corning) to minimize particle bounce. Background air samples were collected from the dynamometer chamber with the same sampling configuration while the dynamometer was not in operation. For the thermal degradation experiments, particles were sampled at 3 L min^{-1} without the MOUDI impactor upstream, as all particles sampled were ultrafine. Background air was sampled from the chamber at the same rate

while no heat was applied to the system. Filter samples were sealed in glass vials with Teflon tape and stored at −4 °C until analysis.

LC-MS was adopted here as it allows for the analysis of very small particulate sample mass, minimizes ion suppression artifacts that have been seen in the analysis of complex organic mixtures with other techniques such as direct infusion,[67] and facilitates molecular identification. Filter samples were extracted in 5 mL acetonitrile (Optima LC-MS grade, Fisher Scientific) and vortex mixed (Thermolyne, model M37615) for 20 min before evaporation to 50 μL under a gentle stream of N_2. A volume of 50 μL ultrapure water (Optima LC-MS grade, Fisher Scientific) was added to the extract to yield a 1 : 1 (v/v) mixture. In addition to filters, the brake pad materials themselves were extracted using the same methodology, but without evaporation due to the presence of sufficient sample mass for analysis. In those experiments, 400 mg of pulverized brake material from a new, unused brake pad were added to 5 mL acetonitrile, corresponding to a final extract concentration of 40 mg mL^{-1} after the addition of 5 mL of water. Extracts were analyzed using an ultrahigh-performance liquid chromatograph (Vanquish UHPLC, Thermo Fisher Scientific) coupled to a photodiode array detector (Vanquish, Thermo Fisher Scientific) followed by a high-resolution Orbitrap mass spectrometer (Q Exactive Plus, Thermo Fisher Scientific) equipped with a heated electrospray ionization inlet (HESI). The UHPLC operating parameters have been described in detail elsewhere,[68] and important details including instrumentation and data analysis with MZmine software are provided in the SI.

3 Results and discussion

3.1 Brake wear particle nucleation

Fig. 1 displays typical UBWP nucleation events observed in the brake dynamometer during harsh braking for ceramic and semi-metallic brake pads. In all experiments, a burst of particles in the lowest measured size bins appears once a certain critical rotor temperature is measured in the cycle (T_{crit}). As noted previously, similar phenomena has been observed in other brake dynamometer experiments that have estimated T_{crit},[39–41] although discussion is lacking on subsequent particle growth characteristics, as this is likely highly dependent on dynamometer chamber and flow conditions. Observations of UBWP nucleation in on-road testing remains challenging, but nucleation-mode particles (as small as 10 nm in diameter) have nevertheless been observed.[69] In the present study, higher rotor temperatures were routinely achieved for semi-metallic brakes (Fig. 1C and Table S1), possibly reflecting differences in thermal conductivity characteristics of the two brake pads. On average, ceramic brake pads exhibited slightly lower T_{crit} values (207 ± 23 °C) than semi-metallic pads (240 ± 14 °C) (Table S1). This is possibly due to the higher concentrations of volatile organic compounds emitted from ceramic brakes upon thermal degradation,[22] allowing vapors to achieve supersaturation more readily. In addition, the extent to which a brake pad resin is cured greatly impacts its thermal stability,[45,60] with less cured resins exhibiting thermal degradation at lower temperatures. Many other factors also affect resin thermal stability, such as the ratio of phenol to formaldehyde used in its synthesis in the case of phenolic resins,[70] as well as the particular curing agents used to set the resin (*e.g.*, HMTA, tannins[71]). The observed differences in T_{crit} values here thus suggest possible manufacturing differences in the resins used in the two pads, in addition to other more obvious compositional differences such as the friction materials. Interestingly, although similar numbers of ultrafine particles are measured ($N_{4–100nm}$, Fig. 1B) ceramic brakes also emit higher concentrations of supermicron particles ($N_{>1μm}$), suggesting nucleation is achieved more readily with ceramic brakes despite the larger condensation sink (*i.e.*, larger surface area) supplied by primary emissions. Such conditions typically prohibit particle nucleation due to the higher probability of new particles and/or their low volatility precursors immediately being scavenging by larger particles upon formation. One possible explanation as to why ceramic brakes are able to achieve nucleation more readily despite this is that these brakes emit high concentrations (>1 ppm) of VOCs at lower temperatures compared to semi-metallic brakes.[22] Fig. S3 provides an expanded view of typical dynamometer experiment profiles, including braking performance (hydraulic pressure, torque) and brake wear particle number-size distributions from the APS. During nucleation, the ceramic brakes experienced more severe brake fade, observed as a reduction in braking torque achieved at a given hydraulic pressure. As resin curing conditions also greatly impact brake fade characteristics,[61] the onset of brake fade as well as the lower T_{crit} values support the hypothesis that the ceramic pad chosen for study contained a less cured resin than the chosen semi-metallic brake pad. In addition, the two brake pads could differ in the amount of other types of resins that are mixed into the formulation for similar purposes, including epoxy resins.[72]

Particle nucleation was also observed in the thermal degradation experiments for both brake pads and the phenolic resin powder (Fig. S4). For the phenolic resin, bursts of ultrafine particles were observed for ∼15–20 min periods at 200, 250, and 300 °C, with peak concentrations in excess of 10^7 cm^{-3} observed for 250 and 300 °C (cured resin). For the brake pads, particle nucleation occurred in ∼5 min bursts at 200 and 250 °C for the ceramic and semi-metallic brake pads, respectively. The lower nucleation temperature observed for ceramic brake pads corroborates the lower T_{crit} values observed from the dynamometer measurements. It is intriguing that particle nucleation in the ceramic brake thermal degradation experiments did not occur until 200 °C, yet half of the dynamometer experiments reported herein exhibited T_{crit} values below this temperature (Table S1). Inhomogeneity of the brake pad composition at different depths is a potential reason for this, possibly explaining the overall variability of T_{crit} from experiment to experiment, with the particular value based on the relative stage of pad wear. zum Hagen *et al.*[39] offered a similar hypothesis after observing T_{crit} increasing upon repeated use of the brake pad. While examining changes in T_{crit} (as well as potential changes in particle composition) across different stages of pad wear is not the subject of the present study, it is nevertheless notable that in a subset of our experiments where

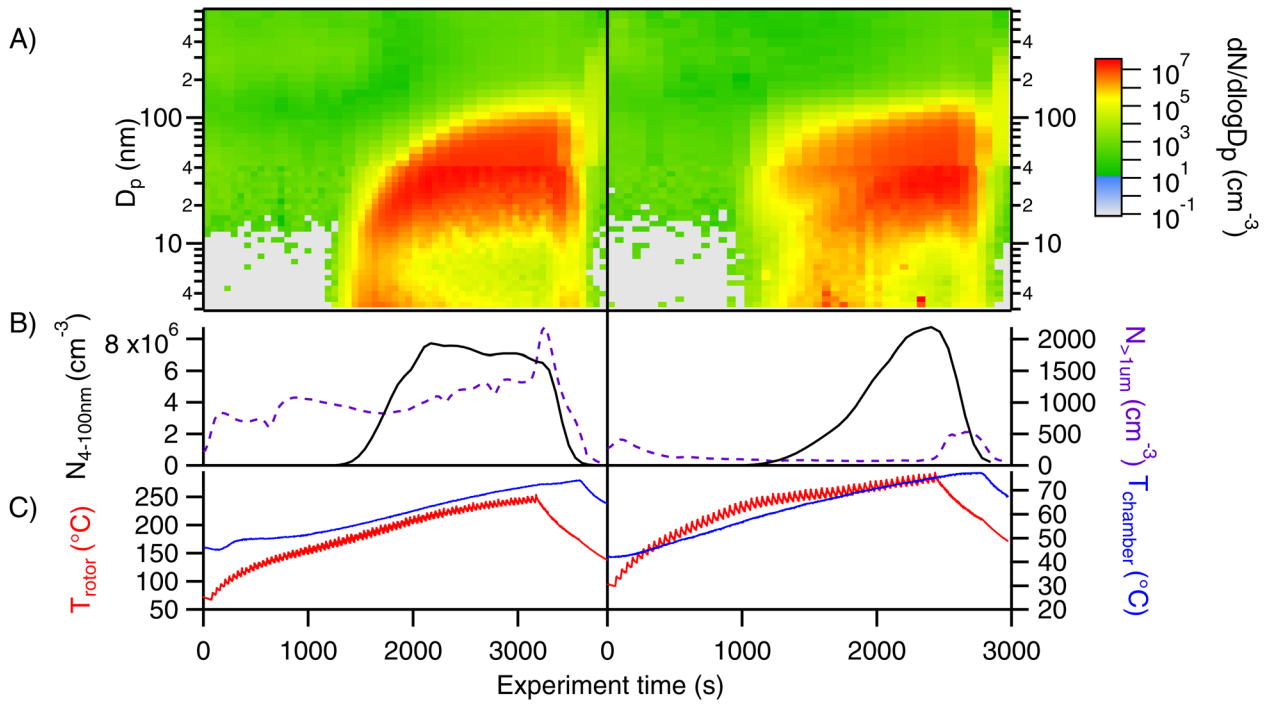

Fig. 1 UBWP nucleation observed in typical brake dynamometer experiments with ceramic (left) and semi-metallic (right) brake pads. Experiment time begins at the initiation of the harsh braking cycle. (A) Overlay of particle number-size distributions obtained from two SMPS systems displaying mobility diameters (D_p) scanned from 4 to 40 nm and 40 to 730 nm. (B) Integrated particle number time series for species detected between mobility diameters 4 to 100 nm (black, solid) and aerodynamic diameters greater than 1000 nm (purple, dashed). (C) Overlay of brake rotor (red) and dynamometer chamber (blue) temperature time series.

the same pads were used regularly in succession, that is one experiment per day, a similar trend where T_{crit} increasing over time was observed for semi-metallic pads (experiments A to C, Table S1), while the opposite trend was observed for ceramic pads (experiments D to I). This suggests that the relationship between T_{crit} and stage of brake wear may differ for different brake pad formulations. The lower T_{crit} values observed in the dynamometer could also potentially be explained by differences in the heating mechanism. Křístková *et al.*[73] found that metals such as iron and copper may serve as catalysts for the thermal degradation reaction of certain phenolic resins. An analogous process may be occurring during frictional contact between the resins used in the ceramic and/or semi-metallic pads and the cast iron rotor, though this should be the subject of future detailed investigations. Additionally, it should be noted that while we use rotor temperatures to report T_{crit}, there is evidence that the actual temperature at the interfacial contact region between brake pad and rotor is much higher than what is measured here, with temperatures reported to be as high as 800 °C.[74–76] The temperatures experienced by the brake pads in the dynamometer could thus be at times far greater than that experienced during the thermal degradation experiments, potentially further explaining the observed variability in T_{crit}.

3.2 TDCIMS characterization

The TDCIMS analysis include experiments conducted with the dynamometer and the thermal degradation of the phenolic resin material. The instrument was not available for the brake pad thermal degradation experiments. Fig. 2 provides an overview of the organic composition of UBWPs generated from the dynamometer experiments as observed with TDCIMS. Table 1 lists the molecular formulae as well as the potential identities for some of the most abundant organic compounds detected in UBWPs with both TDCIMS and LC-MS. Compound IDs are used throughout the text with uppercase letters representing compounds identified in the negative ion mode and lowercase letters for compounds identified in positive ion mode. In general, UBWPs are mostly composed of CHO and CHON organics, with these two compound classes comprising over 70% of the assigned ion intensity in both polarities for both brake types. In the negative ion mode, organic sulfur classes (CHOS, CHONS) contribute a relatively smaller percentage of total assigned intensity, but with nevertheless prominent peaks present specifically in ceramic brake UBWPs, with m/z 353.9925 (neutral formula $C_{13}H_9NO_9S$, compound Q in Table 1) and m/z 354.9765 ($C_{13}H_8O_{10}S$, compound R) being major ions among these. Together, the four compound classes depicted in Fig. 2A account for 99.3% and 99.6% of the assigned ion intensity, or 77.2% and 74.8% of the total (assigned + unassigned) ion intensity attributed to ceramic and semi-metallic brake-derived UBWPs, respectively. Overall compound class abundance did not vary significantly between experiments, with standard deviations varying between 0.1% and 3% depending on the brake type and ion polarity measured. Other assigned negative ions include inorganic SO_x (HSO_4^-, SO_4^-, SO_3^-, SO_2^-, SO_5^-),

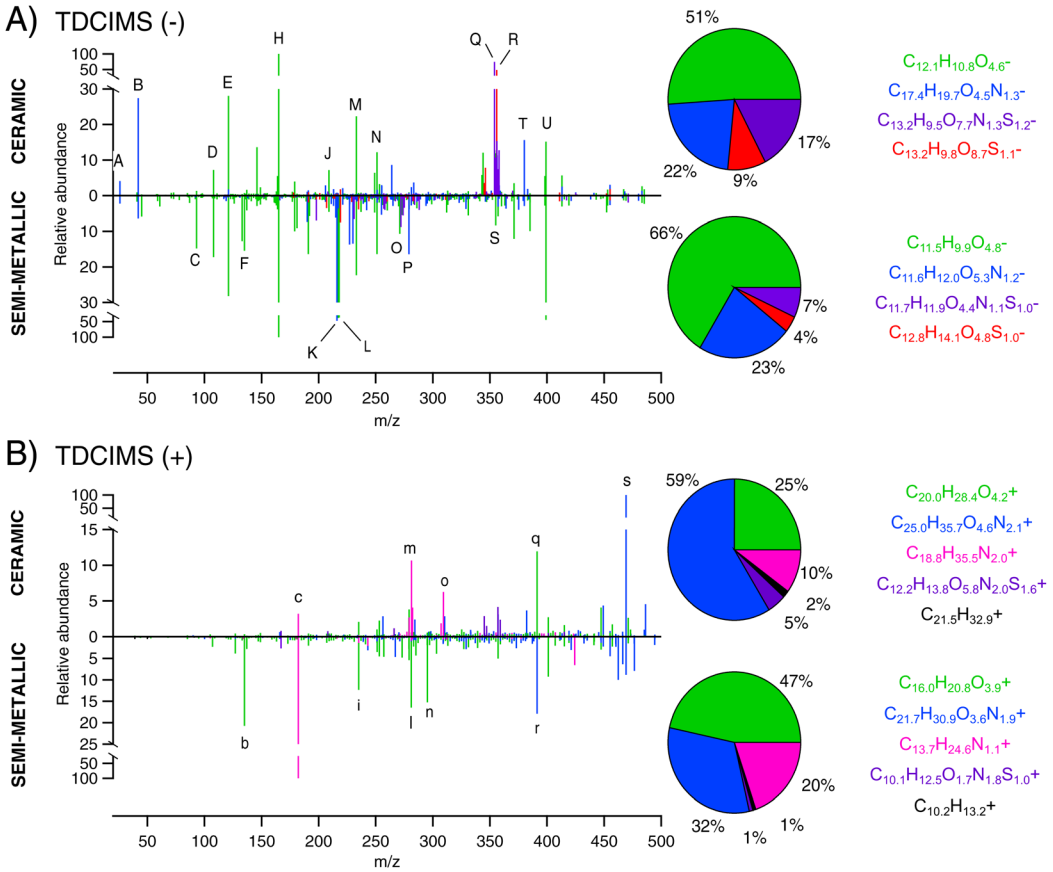

Fig. 2 Overview of UBWP organic composition for ceramic (top of each mirror plot) and semi-metallic (bottom of each mirror plot) brakes as observed with TDCIMS (A) negative and (B) positive ion modes. Colors indicate the assigned compound class: CHO (green), CHON (blue), CHONS (purple), CHOS (red), CHN (pink), and CH (black). Peak height is represented as the average intensity of three experiments. The right side of each spectrum depicts the pie chart of average relative ion abundance of each compound class. At the rightmost of each spectrum is the average ion formulae for each compound class. The molecular formulae of peaks labeled with a letter are presented in Table 1.

whose detection with TDCIMS has previously been attributed to sulfate[62] but may also be related to thermal decomposition of organic sulfur compounds on the Pt wire. SO_x species were more abundant in ceramic brake UBWPs compared to semi-metallic (Fig. S5), but were rather small compared to the signal from total organics, accounting for 0.1% or 0.03% of the total assigned ion intensity in ceramic and semi-metallic brake UBWPs, respectively, after taking into account the relative sensitivity of TDCIMS to SO_x and most organic compounds.[77]

In total, 844 and 777 negative ions with unique molecular formulae were identified with TDCIMS in ceramic and semi-metallic brake UBWPs, respectively. The majority of these compounds matched between the two brake types (706), as did many of the most abundant species. The most abundant negative ion observed in both brake types has the neutral formula $C_8H_6O_4$ (*m*/*z* 165.0193, compound H) and is tentatively identified as an isomer of phthalic acid. One isomer, terephthalic acid, was confirmed by LC-MS (see Section 3.3). Detection of phthalic acid isomers in urban PM has previously been attributed to the photooxidation of polycyclic aromatic hydrocarbons from vehicular exhaust,[78–80] as well as the burning of plastic.[81,82] Its identification here as a major organic species in UBWPs implicates automotive braking as a potentially significant source of phthalic acid isomers as well as other particle-phase aromatic acids. Other CHO compounds abundant in both brake types include $C_7H_6O_2$ (*m*/*z* 121.0295, compound E), $C_{21}H_{20}O_8$ (*m*/*z* 399.1085, compound U), and $C_{13}H_{14}O_4$ (*m*/*z* 233.0819, compound M). Identified abundant CHON species include isocyanic acid (HNCO, *m*/*z* 41.9985, compound B) and hydrocyanic acid (HCN, *m*/*z* 26.0036, compound A). Similar to phthalic acid, detection of HNCO and HCN in urban environments has previously been attributed to combustion processes such as gasoline and biomass burning,[83–85] but was also recently identified in the gas-phase from brake emissions.[22] Due to their volatility, their detection in ultrafine particles with TDCIMS is attributed to the decomposition of larger organic compounds. Other abundant CHON species detected include $C_7H_7NO_7$ (K), $C_{17}H_{13}NO_3$ (P) and $C_{21}H_{19}NO_6$ (T). Given their relatively high degree of unsaturation, it is likely that many CHO and CHON species detected with TDCIMS negative ion mode in both brake types could be derived from phenolic resin binder thermal degradation. Fig. 3 compares the average elemental ratios (X/C) of CHO and CHON compounds detected in UBWPs against nucleated particles generated from heating phenolic resin

Table 1 List of abundant species with suggested identities detected in UBWPs using high resolution mass spectrometry. Identities provided are used to annotate TDCIMS and LC-MS mass spectra included herein. Compound IDs are used throughout the text, where uppercase letters indicate negative ion mode compounds and lowercase letters indicate positive ion mode compounds

(−) Ion mode					(+) Ion mode				
ID	*m/z*	Monoisotopic mass (Da)	Molecular formula	Potential identity	ID	*m/z*	Monoisotopic mass (Da)	Molecular formula	Potential identity
A	26.0036	27.0109	HCN	Hydrogen cyanide	a	109.076	108.0688	$C_6H_8N_2$	Phenylenediamine
B	41.9985	43.0058	HNCO	Isocyanic acid	b	135.0804	134.0732	$C_9H_{10}O$	
C	93.0346	94.0419	C_6H_6O	Phenol	c	182.1903	181.1831	$C_{12}H_{23}N$	Dicyclohexylamine
D	107.0133	108.0211	$C_6H_4O_2$	Quinone	d	188.0931	187.0858	$C_9H_9N_5$	Benzoguanamine
E	121.029	122.0368	$C_7H_6O_2$	Hydroxybenzaldehyde	e	197.0597	196.0524	$C_{13}H_8O_2$	Xanthone
F	135.0446	136.0524	$C_8H_8O_2$		f	207.1591	206.1518	$C_{10}H_{22}O_4$	Triethylene glycol monobutyl ether
G	137.0239	138.0317	$C_7H_6O_3$	Dihydroxybenzaldehyde	g	211.0754	210.0681	$C_{14}H_{10}O_2$	
H	165.0193	166.0266	$C_8H_6O_4$	Terephthalic acid	h	225.091	224.0837	$C_{15}H_{12}O_2$	Flavanone
I	190.0146	191.0219	$C_9H_5NO_4$	Trimellitimide	i	235.0965	234.0892	$C_{13}H_{14}O_4$	
J	209.0456	210.0528	$C_{10}H_{10}O_5$	Unknown phenolic resin product	j	251.1853	250.178	$C_{12}H_{26}O_5$	Tetrapropylene glycol
K	216.015	217.0223	$C_7H_7NO_7$		k	279.0935	278.0863	$C_8H_{14}N_4O_7$	
L	216.999	217.9851	$C_7H_6O_8$		l	281.1172	280.1099	$C_{18}H_{16}O_3$	
M	233.0819	234.0892	$C_{13}H_{14}O_4$		m	281.2951	280.2879	$C_{18}H_{36}N_2$	Unknown diamine
N	251.0925	252.0998	$C_{13}H_{16}O_5$		n	295.2115	294.2042	$C_{14}H_{30}O_6$	Unknown glycol
O	271.0976	272.1049	$C_{16}H_{16}O_4$		o	309.3264	308.3192	$C_{20}H_{40}N_2$	Unknown diamine
P	278.0823	279.0895	$C_{17}H_{13}NO_3$		p	339.1802	338.1729	$C_{18}H_{26}O_6$	
Q	353.9925	354.9998	$C_{13}H_9NO_9S$	Benzothiazole chemistry	q	391.2843	390.2770	$C_{24}H_{38}O_4$	
R	354.9765	355.9838	$C_{13}H_8O_{10}S$	Benzothiazole chemistry	r	391.2955	390.2882	$C_{23}H_{38}N_2O_3$	
S	355.1187	356.1260	$C_{20}H_{20}O_6$		s	469.1969	468.1897	$C_{25}H_{28}N_2O_7$	
T	380.114	381.1212	$C_{21}H_{19}NO_6$						
U	399.1085	400.1158	$C_{21}H_{20}O_8$	Heterodimer of H and N					

powder at three temperatures (200, 250, and 300 °C), as well as the average *m/z* in negative ion mode TDCIMS spectra. Across all experiments, the average H/C ratio maintains a roughly constant value of ~1 for both compound classes, suggesting shared molecular properties/sources between UBWPs and the nucleated phenolic resin particles. It is noteworthy, however, that the average H/C ratio from semi-metallic brake CHO compounds is lower than that observed from the ceramic brakes or from any of the phenolic resin experiments. This is likely driven by the greater relative abundance of highly unsaturated species which are nevertheless plausibly linked to phenolic or epoxy resins as well, including $C_8H_6O_4$ and $C_{21}H_{20}O_8$, with H/C ratios of 0.75 and 0.95, respectively. Average O/C ratios are also similar (~0.3–0.5), but in general are slightly lower for resin particles than UBWPs. Intriguingly, the average O/C ratio increases with nucleation temperature for phenolic resin particles across both compound classes, possibly indicating a greater prevalence of oxidation chemistry at higher temperatures. Given that, on average, semi-metallic brakes nucleated at higher temperatures than ceramic brakes (Table S1), a similar phenomenon may be occurring in UBWPs as O/C ratios are higher in semi-metallic brakes (0.51 ± 0.03 and 0.58 ± 0.01 for CHO and CHON compounds, respectively) than in ceramic brakes (0.48 ± 0.02 and 0.36 ± 0.02). Higher nucleation temperatures may also be associated with greater extents of polymer decomposition, given that the average *m/z* ratios decrease from phenolic resin nucleation temperatures 200 to 300 °C, as well as from ceramic to semi-metallic UBWPs. The phenolic resin experiments at 300 °C were performed after a cool down of the resin to simulate a 'curing' process. It is noteworthy that for CHO compounds, the quantities exhibited at these conditions (O/C, H/C, *m/z*) show the strongest similarity to the corresponding UBWP averages.

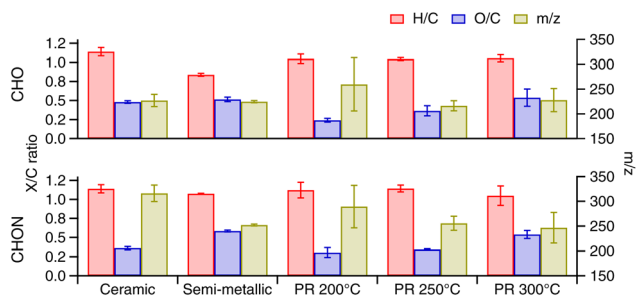

Fig. 3 Comparison of the average H/C (red), O/C (blue), and *m/z* (gold) ratios for CHO (top) and CHON (bottom) compound classes detected with TDCIMS negative ion mode for ceramic and semi-metallic brake UBWPs and nucleated particles generated from the thermal degradation of phenolic resin (PR) at three temperatures. Error bars represent ±1 standard deviation.

Fig. S6 provides an overview of species detected in nucleated phenolic resin particles with TDCIMS operating in negative ion mode. Overall, phenolic resin particles nucleated at 250 °C shared the most molecular formulae with UBWPs, with 626 and 677 matching formulae for ceramic and semi-metallic brake UBWPs, respectively. Phenolic resin particles across all

nucleation temperatures were observed to mostly contain CHO/CHON species, accounting for over 80% of assigned ion intensity. Abundant species detected in phenolic resin particles included isocyanic acid, phenol, and the unknown $C_{13}H_{12}O_2$, all significant species observed in UBWPs as well.

Fig. 2B provides an overview of the positive organic ions detected in UBWPs with TDCIMS. Overall, 1551 and 1324 unique molecular formulae were identified in ceramic and semi-metallic brake UBWPs, respectively, with 1239 of these matching. While CHO and CHON were again the most dominant compound classes observed, the O/C ratios were significantly lower compared to species detected in the negative ion mode, aligning with what is known about the ionization selectivity of protonated water cluster chemical ionization.[86] The most abundant species observed in ceramic brake UBWPs is tentatively assigned the molecular formula $C_{25}H_{28}N_2O_7$ (compound s), and is suggested to be an unknown phenolic oligomer, given its high degree of unsaturation. Similar to negative ion mode, the average elemental ratios of CHO/CHON organics are very close to ratios derived from the phenolic resin particles, with values of ~1.3–1.5 and ~0.2 for H/C and O/C ratios, respectively. Fig. S7 provides an overview of positive ions detected from nucleated phenolic resin particles with TDCIMS including average molecular formulae for the dominant compound classes. Also similar to the negative ion mode, the majority of UBWP molecular formulae matched with nucleated resin particles, sharing nearly 800 peaks with phenolic resin particles nucleating at 200 °C, for instance. Together, these observations suggest that most of the positive ions detected in UBWPs with TDCIMS may also be attributed to resin thermal degradation processes. In addition to oxygenated compounds, CHN species were also abundant, contributing 10–20% to assigned ion abundance in UBWPs. Dominant among observed CHN species, as well as the most abundant compound observed in semi-metallic brake UBWPs, was $C_{12}H_{23}N$ (m/z 182.1903, compound c). This compound is tentatively identified as dicyclohexylamine (DCHA), a recently proposed marker for tire wear PM.[87,88] In tires, DCHA is used in the production of rubber curing agents and as an antioxidant.[89] While DCHA could potentially be used for similar purposes in brake pads, its presence may also be attributed to rubber added to the brake pad formulation, as a common filler material.[90] It is noteworthy that $C_{12}H_{23}N$ was also detected in phenolic resin particles, with peak abundance observed at 200 °C (Fig. S7). Other dominant amines include $C_{18}H_{36}N_2$ (compound m) and $C_{20}H_{40}N_2$ (compound o). Notably, these two diamines have double bond equivalent (DBE) values of 2 like DCHA, suggesting that these unknown species may also be cycloamines. In general, nitrogen-containing species were more abundant in ceramic brake UBWPs than semi-metallic, in line with previous observations that observed more nitrogen-containing gases emitted from ceramic brakes.[22]

3.3 LC-MS characterization

The LC-MS analysis includes experiments conducted with the dynamometer and the thermal degradation from both brake types, as well as the extracts of the brake pad materials themselves. Fig. 4 provides an overview of UBWP organic composition observed using LC-MS. The dataset depicted is of representative samples, while data from a replicate experiment with each brake pad is provided in Fig. S8. Overall, 560 and 1140 unique molecular formulae were identified in ceramic and semi-metallic UBWPs with LC-MS, respectively, with 367 formulae matching between the brake types. Similar to TDCIMS, signal from CHO and CHON species dominated overall ion abundance particularly in the negative ion mode, accounting for 81% or 95% of total ion signal (assigned + unassigned) attributed to ceramic and semi-metallic brake UBWPs, respectively. The average H/C ratios are also similar, ranging from 0.8 to 1 for both compound classes, indicating that phenolic resin and other aromatic constituents of the brake pads are likely key contributors to negative ion signal.

Fig. S9 provides structural identification of some of the most abundant ions detected in both polarities. The most abundant and second most abundant negative ion species observed in semi-metallic and ceramic brake UBWPs, respectively, is identified as terephthalic acid ($C_8H_6O_4$, m/z 165.0193, compound H). Interestingly, this compound may also produce a key ion observed in TDCIMS negative ion mode, although unequivocal identification of organic species with TDCIMS is difficult due to limitations of the mass spectrometer. In the atmosphere, terephthalic acid is associated with plastic burning PM,[81,82] and recently also identified in urban material burning samples, along with phthalic acid.[91] Its presence in UBWPs likely arises from the thermal degradation of phenolic and/or epoxy resins used in the brake pad formulation. Potential use as a marker for brake wear PM in the future would be contingent on knowledge of regional influence from other known sources of the molecule in particles. The most abundant negative ion in ceramic brake UBWPs as detected with LC-MS has the neutral formula $C_{13}H_{16}O_5$ (compound N), and is also tentatively attributed to phenolic and/or epoxy resin thermal degradation. Another species abundant in both brake types is $C_{21}H_{20}O_8$ (compound U), a formula that is also dominant in TDCIMS negative ion mode spectra. While the exact structural identity of the species is unknown, it is possible that it is a dehydration product of the heterodimer of terephthalic acid and the unknown $C_{13}H_{16}O_5$. Given the uniqueness of the formula, compound U could serve as a potential marker if observed in the real atmosphere, warranting further structural investigation in the future. Another species of particular abundance in ceramic brake UBWPs as observed with TDCIMS and LC-MS has the formula $C_{21}H_{19}NO_6$ (compound T), which may be a structurally-related to compound U given their similar H/C ratios, but further experiments (*e.g.*, targeted tandem mass spectrometry) are needed in the future to support this. Other abundant species likely derived from similar sources include $C_7H_6O_2$ (compound E), which we assign to be an unknown isomer of hydroxybenzaldehyde, $C_7H_6O_3$ (compound G), $C_8H_8O_2$ (compound F), and $C_{10}H_{10}O_5$ (compound J).

As observed with TDCIMS, nitrogen-containing compounds dominated the organic composition of UBWPs in the positive ion mode. Overall, 362 unique molecular formulae matched between brake types in this polarity, corresponding to 44% or

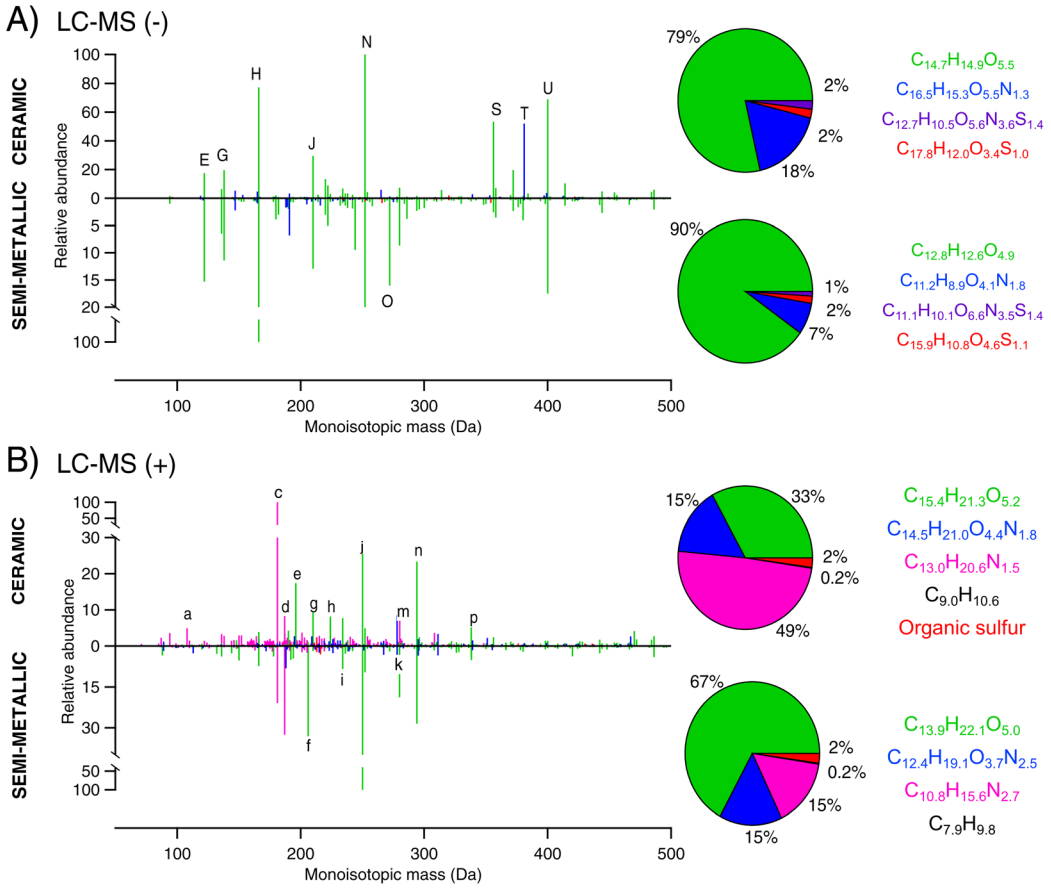

Fig. 4 Representative overview of UBWP organic composition for ceramic (top of each mirror plot) and semi-metallic (bottom of each mirror plot) brake pads as observed with LC-MS (A) negative and (B) positive ion modes. Colors indicate the assigned compound classes: CHO (green), CHON (blue), CHONS (purple), CHN (pink), CH (black). Red is used to represent either CHOS molecules or all organic sulfur species (CHOS, CHONS, CHNS, CHS) detected in the negative ion and positive ion modes, respectively. The right side of each spectrum depicts the pie chart of average relative ion abundance of each compound class, while on the rightmost side is the average molecular formulae for each compound class. The molecular formulae of peaks labeled with a letter are presented in Table 1.

35% of the total number of formulae identified in ceramic (826) and semi-metallic (1027) UBWPs, respectively. The most abundant species observed in ceramic brake UBWPs is identified as DCHA (Fig. S9). This compound is also present in the pad thermal degradation and brake pad extract LC-MS datasets, allowing it to be reasonably assumed that DCHA evaporated from the brake pad material itself. Fig. S10 and S11 provide overviews of the organic composition of brake pad extract and pad thermal degradation products for both brake types, respectively. Given its abundance in UBWPs corroborated with two techniques, as well as its known presence in tire wear particles, this compound is a promising marker for non-exhaust emissions. Another abundant amine with the formula $C_9H_9N_5$ (m/z 188.0931, compound d), is identified as benzoguanamine, a compound used in the production of melamine-formaldehyde resin.[92] This resin is used in brake pad formulations to impart additional thermal stability,[93] but also is traditionally used as a crosslinking agent to improve adhesion in tire rubber.[94] Unlike DCHA, the presence of benzoguanamine has not been widely reported in tire wear or other PM, and thus its potential to serve as a marker for brake wear or other non-exhaust processes remains unexplored. Another aromatic amine was also identified as an isomer of phenylenediamine ($C_6H_8N_2$, m/z 109.0760, compound a), which may also be related to tire rubber additives.

Despite the abundant nitrogen, CHO organics still contributed the most ion abundance to semi-metallic brake UBWPs in LC-MS positive ion mode, similar to negative ion abundance. While resin thermal degradation is likely contributing substantially to CHO species detected in the positive ion mode, with $C_{13}H_{16}O_5$ being abundant in both polarities, a distinct population of highly saturated glycol-like species appear in UBWPs with LC-MS analysis. The first and second most abundant ions detected in semi-metallic brake UBWPs are tentatively identified as tetrapropylene glycol ($C_{12}H_{26}O_5$, m/z 251.1853, compound j) and triethylene glycol monobutyl ether ($C_{10}H_{22}O_4$, m/z 207.1591, compound f), respectively. It is tempting to attribute the presence of these molecules to small amounts of hydraulic brake fluid that may be on the brake caliper or other areas in the dynamometer; however, their abundance in both extracted brake pad material (Fig. S10) as well as particles nucleated from their thermal degradation (Fig. S11)

corroborates their probable origin from brake pads. Although their potential use in brake pads is uncertain, polyethylene glycol was nevertheless reported by Lagel *et al.*[95] as an additive to the synthesis of brake pad resin matrices. Previous studies have identified similar glycol species in dynamometer-generated brake wear particles,[36] in real-world observations of brake lining debris,[96] and road dust PM.[97] Besides glycols, another abundant species was tentatively identified as xanthone (e, see Fig. S9E for identification), suggested to be derived from phenolic or epoxy resin aromatics. Sulfur-containing species represented the smallest fraction of organics observed in both brake types. A notable peak with particular abundance in ceramic brake UBWPs is nevertheless tentatively identified as an isomer of phenylbenzothiazole ($C_{13}H_9NS$, m/z 212.0529, Fig. S12). Benzothiazole and its derivatives are used in the rubber vulcanization process and have been used previously as markers for tire wear PM,[98] and may be observed here from rubber filler materials present in the brake pad formulation. It is noteworthy that the two dominant sulfur-containing species detected in ceramic brake UBWPs with TDCIMS negative ion mode ($C_{13}H_9NO_9S$ and $C_{13}H_9O_{10}S$) share a similar formula as phenylbenzothiazole. Recent investigations have reported on the potential for benzothiazoles to undergo atmospheric oxidation.[99–101] Benzothiazole oxidation may also occur during automotive braking, though future work is needed to comment conclusively.

While similarities in the organic composition of particles nucleated from the thermal degradation of the brake pads and the composition of the brake pads themselves were assessed to help identify the source of organics in UBWPs, the differences between the datasets are in some ways more intriguing. As expected, a significant number of molecular formulae matched between the datasets. In the negative ion mode, for instance, 50 molecular formulae matched between ceramic brake UBWPs and the thermal degradation particles, while 109 matched between UBWPs and the brake pad extract itself. More overlap was observed for semi-metallic brake UBWPs, with 156 and 157 formulae matching with thermal degradation particles and brake pad extract, respectively. Despite their similarities, significant differences were observed in the oxidation states and degrees of unsaturation of the organics observed. Fig. 5 depicts the negative ion mode distribution of double bond equivalents and carbon oxidation states in CHO-containing molecules detected in UBWPs and thermal degradation particles for both brake types, while Fig. S13 compares UBWPs to brake pad extracts. In general, species are more oxidized, more unsaturated, and heavier in UBWPs compared to both other datasets. The differences are least obvious when comparing the ceramic brake extract with the UBWP organics (Fig. S13), although similar differences are still apparent when comparing the average CHO molecular formulae between the two datasets (Fig. 4 and S10). Differences between the extract and UBWP organics imply that chemistry has led to the presence of ultrafine particles in the dynamometer, with probable reaction pathways being the friction-induced pad thermal degradation and subsequent oxidation of previously un-extractable polymeric material. The observed differences between UBWPs and

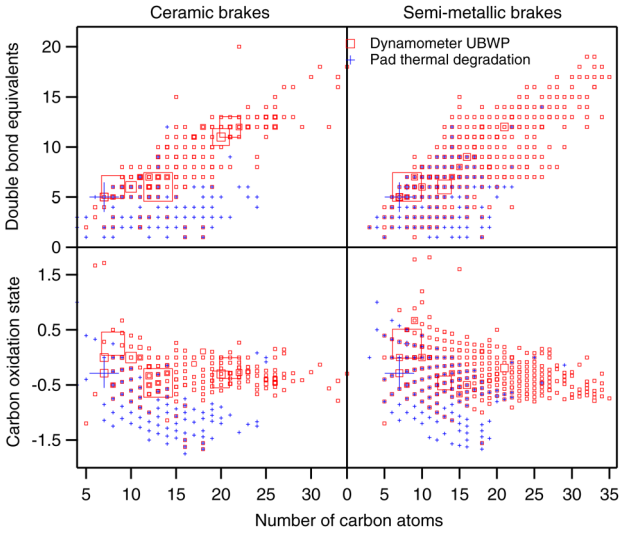

Fig. 5 Distribution of double bond equivalents (top) and carbon oxidation states (bottom) in CHO organic compounds identified in ceramic (left) and semi-metallic (right) brake UBWPs (red squares) and pad thermal degradation particles from both brake types (blue crosses). Marker size corresponds to relative ion abundance.

thermal degradation particles is somewhat more ambiguous. As previously mentioned, although the temperatures probed in the thermal degradation experiments are within range of the T_{crit} values observed in our dynamometer measurements, there is strong evidence that the actual interfacial temperature between the brake pad and rotor is much higher.[74–76] Thus, a probable explanation for the prevalence of larger, more oxidized compounds in UBWPs is that the temperatures experienced by the brake pad in the dynamometer exceeded those experienced in the thermal degradation experiments, inducing greater extents of chemical processing. Species can also undergo oxidation due to tribological-related processes associated with automotive braking.[102]

Larger, more unsaturated species were also observed in the positive ion mode compared to the thermal degradation experiments. Fig. 6 plots the Kendrick mass defect of CHO species detected in the positive ion mode for UBWPs generated in the dynamometer and nucleated from thermal degradation for both brake types. While saturated, glycol-like species are abundant in each dataset (Fig. 6 cyan cluster), only dynamometer-generated particles contain a second population of CHO organics that are larger and more unsaturated. This again may be a consequence of the higher temperatures likely experienced by the brake pad during the dynamometer experiments, as resin material has been shown to release hydrogen at high temperatures,[103] possibly resulting in the formation of double bonds in the emitted oligomeric species. Additionally, both brake types were previously shown to emit hydrogen gas (H_2) under the same braking conditions,[22] supporting the existence of this reaction pathway.

The molecular volatility of organics detected in UBWPs was estimated using a molecular corridor parameterization[104] to determine what types of compounds are likely key to particle

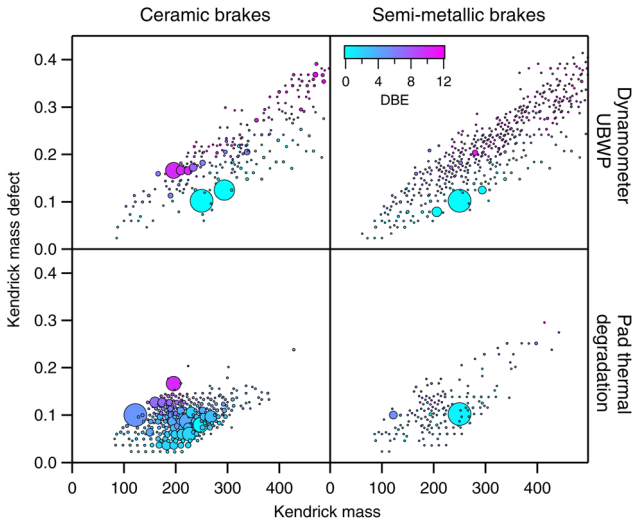

Fig. 6 CH_2 Kendrick mass defect diagrams of CHO organics detected in positive ion mode in dynamometer-generated UBWPs (top) and the pad thermal degradation particles (bottom) for ceramic (left) and semi-metallic (right) brake types. Marker size corresponds to relative ion abundance while marker color corresponds to the number of double bond equivalents of the species detected.

nucleation. Fig. 7 depicts the volatility distributions for the most abundant compound classes observed in ceramic brake UBWPs in both polarities, and compares this to distributions observed in thermal degradation particles as well as species extracted from the raw brake pad material. Fig. S14 provides the same as observed for semi-metallic brake UBWPs. Compounds shown are binned into one of four volatility classes: intermediate volatility organic compounds (IVOCs, having saturation mass concentrations C_0 between 300 and 3×10^6 μg m^{-3}), semi-volatile organic compounds (SVOCs, $0.3 < C_0 < 300$ μg m^{-3}), low volatility organic compounds (LVOCs, $3 \times 10^{-4} < C_0 < 0.3$ μg m^{-3}), or extremely low volatility organic compounds (ELVOCs, $C_0 < 3 \times 10^{-4}$ μg m^{-3}).[105,106] UBWP species exhibit a wide array of volatilities compared to species derived from thermal degradation and brake pad extraction, possibly due to the greater extents of functionalization and oligomerization of emitted species. Most of the species observed from the thermal degradation experiments as well as from brake pad extraction are classified as IVOCs, while a significant fraction of compounds are binned into the LVOC and ELVOC classes in dynamometer-generated UBWPs. CHO and CHON species dominate these lower volatility classes, with CHON being particularly abundant in the negative ion ELVOC fraction. This indicates that these species, mostly larger ($m/z > 200$) oligomers likely derived from the decomposition of various resins used in the pad formulation, are significant contributors to UBWP formation and growth. The greater abundance of oxygenates suggests a distinct chemical mechanism specific to the automotive braking and resin degradation processes that is difficult to reproduce by simple heating of the brake pad. Likely differences in the actual temperatures experienced by the brake pads and in the chamber dynamics between the two experiment types prevents a definitive comparison here. Compared to oxygenated species, detected amines (CHN) were more volatile, although it is noted that the adopted parameterization has been shown to overestimate the volatility of nitrogen-containing species.[107] In addition to highlighting the potential existence of unique chemical pathways, comparison of the oxidation states, double bond equivalents, and molecular volatilities of UBWPs with the other datasets also underscores the importance of utilizing a brake dynamometer to simulate real-world braking emissions as opposed to other strategies such as heating the brake pad without friction.

3.4 Environmental impacts

The organic species identified herein are expected to influence UBWPs ability to impact climate and visibility. Due to their low

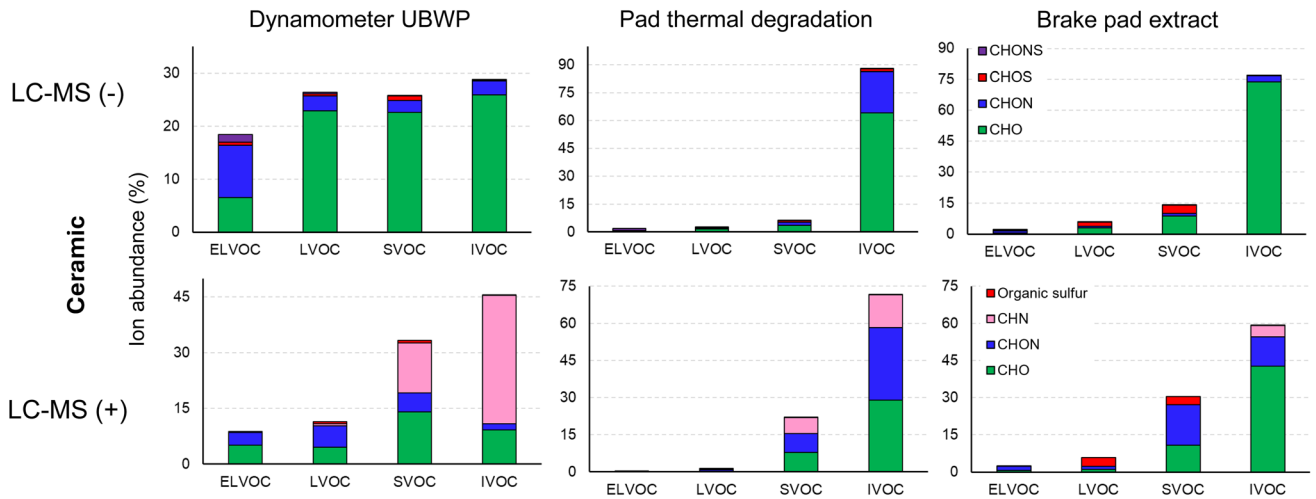

Fig. 7 Molecular volatility distributions of organic species detected in LC-MS negative ion (top) and positive ion (bottom) modes for ceramic brakes in dynamometer-generated UBWPs (left), nucleated thermal degradation particles (middle), and brake pad extract (right). Color indicates assigned compound class. Ion abundance (expressed as a percentage) is relative to each distribution. Fig. S14 depicts the volatility distributions as observed in semi-metallic brake experiments.

volatility, many of the species emitted can participate in particle formation and growth in the atmosphere, potentially adding significantly to cloud condensation nuclei in near-highway environments. In addition, many of the organics observed have the potential to interact with sunlight, directly impacting UBWP climatic properties. Fig. 8 shows the distribution of chromophores present in dynamometer-generated UBWPs absorbing between the wavelengths 250–400 nm for both brake types studied. At these wavelengths, UBWPs can not only scatter but also absorb incident solar radiation and thereby contribute to aerosol climate forcing. Future work dedicated to understanding the photochemistry of the UBWP organic matrix is needed to fully appreciate the climatic implications of their emission.

Further studying the organic composition of BWPs is also crucial to understanding the toxicological implications of their inhalation in real urban environments. Due to their small size, UBWPs pose a particular health risk as they can enter the bloodstream.[28] Given that many of the species observed here are likely oxidized aromatic compounds, it is reasonable to suspect that UBWPs are generally toxic given what is known regarding aerosol systems comprised of similar species such as vehicular exhaust and biomass burning emissions.[108] Aromatic amines, such as the identified phenylenediamine, are also known to be toxic when inhaled,[109] and their presence in tire wear particles is implicated in their toxicity to humans, plants, and aquatic organisms.[110] Indeed, our findings here suggest that previous investigations attributing the presence of some of these chemicals in the environment to tire wear may also have been contributed by brake wear processes. BWP species are already implicated in the contamination of soil[111] and aquatic[112] systems chiefly through deposition in stormwater runoff, but emissions of ultrafine particles imply that these environmental impacts may extend well beyond near-highway environments *via* long-range atmospheric transport, emphasizing the need for better emission quantification. Building quantitative source profiles of organic speciation based on real-world driving cycles such as the world harmonized light-duty vehicle test[113] will greatly enhance our understanding of the potential environmental burden of UBWP species.

The identification of several tire-related species including DCHA in UBWPs puts into question their potential to serve as tire wear markers with sufficient specificity. They nevertheless may serve as markers for non-exhaust processes in general, though future work is needed to quantify their presence in brake emissions for a larger diversity of brake types. Several oligomers implicated in the thermal degradation of phenolic resin as discussed here such as $C_{13}H_{16}O_5$ and $C_{21}H_{20}O_8$ should also be investigated as potential markers for UBWP emissions. Given that many species present in the nucleated UBWPs studied here are likely derived from phenolic resin material, as an abundant source of unsaturated CHO/CHON organics, a promising future direction is the isolation and structural characterization of the BWP-related oligomers derived from this source. The key challenge in unequivocal marker identification going forward will be in determining the chemical similarity in the UBWPs emitted from one brake pad to the next, a problem likely needed to be overcome before substantial regulation of brake wear emissions in general can be enacted in the future.

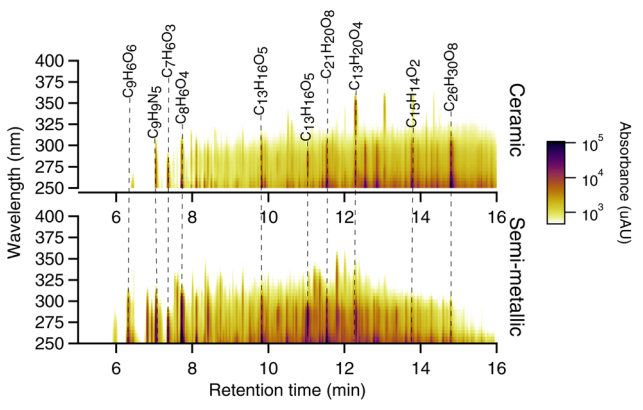

Fig. 8 LC chromatograms showing the distribution of chromophores absorbing between the wavelengths 250–400 nm in ceramic brake (top) and semi-metallic brake (bottom) UBWPs. Overlaid are suggested molecular formulae for significantly absorbing species.

Author contributions

J. N. S. and B. J. F.-P. secured funding and conceived research concept. A. E. T., V. P., M. L., B. R., M. E. C., and P. S. B. performed research. A. E. T. analyzed and visualized data under the supervision of J. N. S. A. E. T. prepared the manuscript with contributions from all authors.

Conflicts of interest

There are no conflicts to declare.

Data availability

Data for this article,[114] including peak lists for all of the mass spectrometry datasets presented herein, are publicly available and archived at **https://doi.org/10.5061/dryad.tmpg4f5bm**.

Supplementary information: dynamometer description; liquid chromatography – mass spectrometry parameters and analysis. Supporting figures: Fig. S1, schematic of the brake dynamometer experimental layout; Fig. S2, overview of the thermal degradation experimental layout; Fig. S3, typical profiles of brake dynamometer experimental variables; Fig. S4, particle size distributions and temperature ramps for the thermal degradation of phenolic resin and brake pad linings. Fig. S5, TDCIMS thermograms of SO_x species; Fig. S6, overview of the organic composition of particles nucleated form the thermal degradation of phenolic resin powder observed with TDCIMS (−); Fig. S7, overview of the organic composition of particles nucleated form the thermal degradation of phenolic resin powder observed with TDCIMS (+); Fig. S8, overview of UBWP organic composition for replicate ceramic and semi-metallic brake experiments observed with LC-MS; Fig S9, structural identification of the most abundant species observed in LC-MS; Fig. S10, overview of the organic composition of

ceramic and semi-metallic brake pad extracts observed with LC-MS; Fig. S11, overview of the organic composition of particles nucleated from the thermal degradation of ceramic and semi-metallic brake pad linings observed with LC-MS; Fig. S12, extracted ion chromatograms of *m*/*z* 212.0529; Fig. S13, distribution of double bond equivalents and carbon oxidation states in CHO organic compounds identified in ceramic and semi-metallic UBWP and brake extracts; Fig. S14, molecular volatility distributions of organic species detected in the negative and positive ion modes for semi-metallic UBWPs. Supporting Tables: Table S1, summary of braking and temperature conditions for the dynamometer experiments; Table S2, instrument parameters for the Orbitrap mass spectrometer; Table S3, MZmine batch mode processing parameters used for the analysis of LC-MS data. See DOI: **https://doi.org/10.1039/d5em00654f**.

Acknowledgements

This research was supported by the California Department of Justice (no. AERTF-221620) and National Science Foundation (no. 2327825). This material is based upon work supported by the National Science Foundation under award no. 2324901. The authors would like to gratefully acknowledge Mark Steinborn, Shane Embleton, and Dustin Cedarholm of the UCI physical sciences machine shop for their support in the operation of the dynamometer used in the experiments described herein.

References

1 L. E. Erickson, G. L. Newmark, M. J. Higgins and Z. Wang, Nitrogen oxides and ozone in urban air: A review of 50 plus years of progress, *Environ. Prog. Sustainable Energy*, 2020, **39**, e13484.
2 F. Karagulian, C. A. Belis, C. F. C. Dora, A. M. Prüss-Ustün, S. Bonjour, H. Adair-Rohani, *et al.*, Contributions to cities' ambient particulate matter (PM): A systematic review of local source contributions at global level, *Atmos. Environ.*, 2015, **120**, 475–483.
3 F. Amato, F. R. Cassee, H. A. C. D. van der Gon, R. Gehrig, M. Gustafsson, W. Hafner, *et al.*, Urban air quality: The challenge of traffic non-exhaust emissions, *J. Hazard. Mater.*, 2014, **275**, 31–36.
4 P. Pant and R. M. Harrison, Estimation of the contribution of road traffic emissions to particulate matter concentrations from field measurements: A review, *Atmos. Environ.*, 2013, **77**, 78–97.
5 H. Boogaard, A. P. Patton, R. W. Atkinson, J. R. Brook, H. H. Chang, D. L. Crouse, *et al.*, Long-term exposure to traffic-related air pollution and selected health outcomes: A systematic review and meta-analysis, *Environ. Int.*, 2022, **164**, 107262.
6 K. Zhang and S. Batterman, Air pollution and health risks due to vehicle traffic, *Sci. Total Environ.*, 2013, **450–451**, 307–316.
7 B. Antonczak, T. M. Thompson, M. W. DePaola and G. Rowangould, 2020 Near-roadway population census, traffic exposure and equity in the United States, *Transp. Res., Part D: Transp. Environ.*, 2023, **125**, 103965.
8 S. E. Chambliss, C. P. R. Pinon, K. P. Messier, B. LaFranchi, C. R. Upperman, M. M. Lunden, *et al.*, Local- and regional-scale racial and ethnic disparities in air pollution determined by long-term mobile monitoring, *Proc. Natl. Acad. Sci. U. S. A.*, 2021, **118**, e2109249118.
9 Y. M. Park and M. P. Kwan, Understanding Racial Disparities in Exposure to Traffic-Related Air Pollution: Considering the Spatiotemporal Dynamics of Population Distribution, *Int. J. Environ. Res. Public Health*, 2020, **17**, 908.
10 G. Pratt, M. Vadali, D. Kvale and K. Ellickson, Traffic, Air Pollution, Minority and Socio-Economic Status: Addressing Inequities in Exposure and Risk, *Int. J. Environ. Res. Public Health*, 2015, **12**, 5355–5372.
11 G. T. Drozd, Y. Zhao, G. Saliba, B. Frodin, C. Maddox, R. J. Weber, *et al.*, Time Resolved Measurements of Speciated Tailpipe Emissions from Motor Vehicles: Trends with Emission Control Technology, Cold Start Effects, and Speciation, *Environ. Sci. Technol.*, 2016, **50**, 13592–13599.
12 Y. Pang, M. Fuentes and P. Rieger, Trends in selected ambient volatile organic compound (VOC) concentrations and a comparison to mobile source emission trends in California's South Coast Air Basin, *Atmos. Environ.*, 2015, **122**, 686–695.
13 T. V. Johnson, Review of Vehicular Emissions Trends, *SAE Int. J. Engines*, 2015, **8**, 2015–010993.
14 J. C. Fussell, M. Franklin, D. C. Green, M. Gustafsson, R. M. Harrison, W. Hicks, *et al.*, A Review of Road Traffic-Derived Non-Exhaust Particles: Emissions, Physicochemical Characteristics, Health Risks, and Mitigation Measures, *Environ. Sci. Technol.*, 2022, **56**, 6813–6835.
15 A. Piscitello, C. Bianco, A. Casasso and R. Sethi, Non-exhaust traffic emissions: Sources, characterization, and mitigation measures, *Sci. Total Environ.*, 2021, **766**, 144440.
16 R. M. Harrison, J. Allan, D. Carruthers, M. R. Heal, A. C. Lewis, B. Marner, *et al.*, Non-exhaust vehicle emissions of particulate matter and VOC from road traffic: A review, *Atmos. Environ.*, 2021, **262**, 118592.
17 R. M. Harrison, A. M. Jones, J. Gietl, J. Yin and D. C. Green, Estimation of the Contributions of Brake Dust, Tire Wear, and Resuspension to Nonexhaust Traffic Particles Derived from Atmospheric Measurements, *Environ. Sci. Technol.*, 2012, **46**, 6523–6529.
18 S. Lawrence, R. Sokhi, K. Ravindra, H. Mao, H. D. Prain and I. D. Bull, Source apportionment of traffic emissions of particulate matter using tunnel measurements, *Atmos. Environ.*, 2013, **77**, 548–557.
19 N. Bukowiecki, P. Lienemann, M. Hill, M. Furger, A. Richard, F. Amato, *et al.*, PM10 emission factors for non-exhaust particles generated by road traffic in an urban street canyon and along a freeway in Switzerland, *Atmos. Environ.*, 2010, **44**, 2330–2340.
20 M. E. Cooke, M. Dam, L. M. Wingen, V. Perraud, A. E. Thomas, B. Rojas, *et al.*, Emissions of Nitrous Acid,

Nitryl Chloride, and Dinitrogen Pentoxide Associated with Automotive Braking, *Environ. Sci. Technol.*, 2025, **59**, 9167–9177.

21 O. Durif, L. Bard, K. Elihn, B. Nozière, U. Olofsson and S. S. Steimer, Emissions of Volatile Organic Compounds from Brake Wear and Their Role in Ultrafine Particle Nucleation, *ACS ES&T Air*, 2025, **2**, 1308–1314.

22 V. Perraud, D. R. Blake, L. M. Wingen, B. Barletta, P. S. Bauer, J. Campos, *et al.*, Unrecognized volatile and semi-volatile organic compounds from brake wear, *Environ. Sci.: Processes Impacts*, 2024, **26**, 928–941.

23 D. Plachá, M. Vaculík, M. Mikeska, O. Dutko, P. Peikertová, J. Kukutschová, *et al.*, Release of volatile organic compounds by oxidative wear of automotive friction materials, *Wear*, 2017, **376–377**, 705–716.

24 A. Patel, S. Aggarwal, L. Bard, O. Durif, M. Introna, A. T. Juárez-Facio, *et al.*, Gaseous emissions from brake wear can form secondary particulate matter, *Sci. Rep.*, 2024, **14**, 23253.

25 N. Rietmann, B. Hügler and T. Lieven, Forecasting the trajectory of electric vehicle sales and the consequences for worldwide CO_2 emissions, *J. Cleaner Prod.*, 2020, **261**, 121038.

26 R. M. Rubio, D. A. Herman, J. Bautista, E. Choy, B. Bliss, L. M. Wingen, *et al.*, Sex-dependent toxic effects of ceramic and semi-metallic brake wear particles, *Ecotoxicol. Environ. Saf.*, 2025, in review.

27 T. Fang, S. Kapur, K. C. Edwards, H. Hagino, L. M. Wingen, V. Perraud, *et al.*, Aqueous OH Radical Production by Brake Wear Particles, *Environ. Sci. Technol. Lett.*, 2024, **11**, 315–322.

28 M. E. Gerlofs-Nijland, B. G. H. Bokkers, H. Sachse, J. J. E. Reijnders, M. Gustafsson, A. J. F. Boere, *et al.*, Inhalation toxicity profiles of particulate matter: a comparison between brake wear with other sources of emission, *Inhalation Toxicol.*, 2019, **31**, 89–98.

29 A. Kazimirova, P. Peikertova, M. Barancokova, M. Staruchova, J. Tulinska, M. Vaculik, *et al.*, Automotive airborne brake wear debris nanoparticles and cytokinesis-block micronucleus assay in peripheral blood lymphocytes: A pilot study, *Environ. Res.*, 2016, **148**, 443–449.

30 P. Peikertova, M. Kuricova, A. Kazimirova, J. Tulinska, M. Barancokova, A. Liskova, *et al.*, Toxicity of the Airborne Brake Wear Debris, *SAE Int. J. Mater. Manuf.*, 2016, **10**, 2016–011914.

31 J. Kukutschová, V. Roubíček, K. Malachová, Z. Pavlíčková, R. Holuša, J. Kubačková, *et al.*, Wear mechanism in automotive brake materials, wear debris and its potential environmental impact, *Wear*, 2009, **267**, 807–817.

32 V. Forest and J. Pourchez, Biological effects of brake wear particles in mammalian models: A systematic review, *Sci. Total Environ.*, 2023, **905**, 167266.

33 B. Lopez, X. Wang, L. W. A. Chen, T. Ma, D. Mendez-Jimenez, L. C. Cobb, *et al.*, Metal contents and size distributions of brake and tire wear particles dispersed in the near-road environment, *Sci. Total Environ.*, 2023, **883**, 163561.

34 P. G. Sanders, N. Xu, T. M. Dalka and M. M. Maricq, Airborne Brake Wear Debris: Size Distributions, Composition, and a Comparison of Dynamometer and Vehicle Tests, *Environ. Sci. Technol.*, 2003, **37**, 4060–4069.

35 B. D. Garg, S. H. Cadle, P. A. Mulawa, P. J. Groblicki, C. Laroo and G. A. Parr, Brake Wear Particulate Matter Emissions, *Environ. Sci. Technol.*, 2000, **34**, 4463–4469.

36 C. Alves, M. Evtyugina, A. Vicente, E. Conca and F. Amato, Organic profiles of brake wear particles, *Atmos. Res.*, 2021, **255**, 105557.

37 M. L. Feo, M. Torre, P. Tratzi, F. Battistelli, L. Tomassetti, F. Petracchini, *et al.*, Laboratory and on-road testing for brake wear particle emissions: a review, *Environ. Sci. Pollut. Res.*, 2023, **30**, 100282–100300.

38 T. Grigoratos and G. Martini, Brake wear particle emissions: a review, *Environ. Sci. Pollut. Res.*, 2015, **22**, 2491–2504.

39 F. H. F. zum Hagen, M. Mathissen, T. Grabiec, T. Hennicke, M. Rettig, J. Grochowicz, *et al.*, Study of Brake Wear Particle Emissions: Impact of Braking and Cruising Conditions, *Environ. Sci. Technol.*, 2019, **53**, 5143–5150.

40 H. G. Namgung, J. B. Kim, S. H. Woo, S. Park, M. Kim, M. S. Kim, *et al.*, Generation of Nanoparticles from Friction between Railway Brake Disks and Pads, *Environ. Sci. Technol.*, 2016, **50**, 3453–3461.

41 J. Kukutschová, P. Moravec, V. Tomášek, V. Matějka, J. Smolík, J. Schwarz, *et al.*, On airborne nano/micro-sized wear particles released from low-metallic automotive brakes, *Environ. Pollut.*, 2011, **159**, 998–1006.

42 M. Mathissen, V. Scheer, R. Vogt and T. Benter, Investigation on the potential generation of ultrafine particles from the tire–road interface, *Atmos. Environ.*, 2011, **45**, 6172–6179.

43 A. Borawski, Conventional and unconventional materials used in the production of brake pads – review, *Sci. Eng. Compos. Mater.*, 2020, **27**, 374–396.

44 D. Chan and G. W. Stachowiak, Review of automotive brake friction materials, *Proc. Inst. Mech. Eng., Part D*, 2004, **218**, 953–966.

45 C. Menapace, M. Leonardi, M. Secchi, A. Bonfanti, S. Gialanella and G. Straffelini, Thermal behavior of a phenolic resin for brake pad manufacturing, *J. Therm. Anal. Calorim.*, 2019, **137**, 759–766.

46 P. Nawangsari, Jamasri and H. S. B. Rochardjo, Effect of Phenolic Resin on Density, Porosity, Hardness, Thermal Stability, and Friction Performance as A Binder in Non-Asbestos Organic Brake Pad, *IOP Conf. Ser.: Mater. Sci. Eng.*, 2019, **547**, 012012.

47 A. Tamayo, F. Rubio, R. Pérez-Aparicio, L. Saiz-Rodríguez and J. Rubio, Preparation and Properties of Sustainable Brake Pads with Recycled End-of-Life Tire Rubber Particles, *Polymers*, 2021, **13**, 3371.

48 A. Stanard, T. DeFries, C. Palacios and S. Kishan, *Brake and Tire Wear Emissions Project 17RD016*, Eastern Research Group, 2021.

49 J. K. Gietl, R. Lawrence, A. J. Thorpe and R. M. Harrison, Identification of brake wear particles and derivation of a quantitative tracer for brake dust at a major road, *Atmos. Environ.*, 2010, **44**, 141–146.
50 A. Iijima, K. Sato, K. Yano, M. Kato, K. Kozawa and N. Furuta, Emission Factor for Antimony in Brake Abrasion Dusts as One of the Major Atmospheric Antimony Sources, *Environ. Sci. Technol.*, 2008, **42**, 2937–2942.
51 L. Calderón-Garcidueñas and A. Ayala, Air Pollution, Ultrafine Particles, and Your Brain: Are Combustion Nanoparticle Emissions and Engineered Nanoparticles Causing Preventable Fatal Neurodegenerative Diseases and Common Neuropsychiatric Outcomes?, *Environ. Sci. Technol.*, 2022, **56**, 6847–6856.
52 F. L. Nassan, C. Wang, R. S. Kelly, J. A. Lasky-Su, P. S. Vokonas, P. Koutrakis, *et al.*, Ambient $PM_{2.5}$ species and ultrafine particle exposure and their differential metabolomic signatures, *Environ. Int.*, 2021, **151**, 106447.
53 D. E. Schraufnagel, The health effects of ultrafine particles, *Exp. Mol. Med.*, 2020, **52**, 311–317.
54 J. L. Allen, G. Oberdorster, K. Morris-Schaffer, C. Wong, C. Klocke, M. Sobolewski, *et al.*, Developmental neurotoxicity of inhaled ambient ultrafine particle air pollution: Parallels with neuropathological and behavioral features of autism and other neurodevelopmental disorders, *NeuroToxicology*, 2017, **59**, 140–154.
55 D. M. Westervelt, J. R. Pierce, I. Riipinen, W. Trivitayanurak, A. Hamed, M. Kulmala, *et al.*, Formation and growth of nucleated particles into cloud condensation nuclei: model–measurement comparison, *Atmos. Chem. Phys.*, 2013, **13**, 7645–7663.
56 J. Merikanto, D. V. Spracklen, G. W. Mann, S. J. Pickering and K. S. Carslaw, Impact of nucleation on global CCN, *Atmos. Chem. Phys.*, 2009, **9**, 8601–8616.
57 A. E. Thomas, P. S. Bauer, M. Dam, V. Perraud, L. M. Wingen and J. N. Smith, Automotive braking is a source of highly charged aerosol particles, *Proc. Natl. Acad. Sci. U. S. A.*, 2024, **121**, e2313897121.
58 T. Grigoratos, C. Agudelo, J. Grochowicz, S. Gramstat, M. Robere, G. Perricone, *et al.*, Statistical Assessment and Temperature Study from the Interlaboratory Application of the WLTP–Brake Cycle, *Atmosphere*, 2020, **11**, 1309.
59 F. F. Binda, V. de Alvarenga Oliveira, C. A. Fortulan, L. B. Palhares and C. G. dos Santos, Friction elements based on phenolic resin and slate powder, *J. Mater. Res. Technol.*, 2020, **9**, 3378–3383.
60 H. Jang, in *Brake Friction Materials*, Springer US, 2013, pp. 263–273.
61 R. C. Dante, *Handbook of Friction Materials and Their Applications*, Woodhead Publishing, 2015.
62 J. N. Smith, K. F. Moore, P. H. McMurry and F. L. Eisele, Atmospheric Measurements of Sub-20 nm Diameter Particle Chemical Composition by Thermal Desorption Chemical Ionization Mass Spectrometry, *Aerosol Sci. Technol.*, 2004, **38**, 100–110.
63 D. Voisin, J. N. Smith, H. Sakurai, P. H. McMurry and F. L. Eisele, Thermal Desorption Chemical Ionization Mass Spectrometer for Ultrafine Particle Chemical Composition, *Aerosol Sci. Technol.*, 2003, **37**, 471–475.
64 S. H. Zhang and R. C. Flagan, Resolution of the radial differential mobility analyzer for ultrafine particles, *J. Aerosol Sci.*, 1996, **27**, 1179–1200.
65 H. Stark, R. L. N. Yatavelli, S. L. Thompson, J. R. Kimmel, M. J. Cubison, P. S. Chhabra, *et al.*, Methods to extract molecular and bulk chemical information from series of complex mass spectra with limited mass resolution, *Int. J. Mass Spectrom.*, 2015, **389**, 26–38.
66 V. A. Marple, K. L. Rubow and S. M. Behm, A Microorifice Uniform Deposit Impactor (MOUDI): Description, Calibration, and Use, *Aerosol Sci. Technol.*, 1991, **14**, 434–446.
67 I. Kourtchev, P. Szeto, I. O'Connor, O. A. M. Popoola, W. Maenhaut, J. Wenger, *et al.*, Comparison of Heated Electrospray Ionization and Nanoelectrospray Ionization Sources Coupled to Ultra-High-Resolution Mass Spectrometry for Analysis of Highly Complex Atmospheric Aerosol Samples, *Anal. Chem.*, 2020, **92**, 8396–8403.
68 A. E. Thomas, H. S. Glicker, A. B. Guenther, R. Seco, O. V. Bustillos, J. Tota, *et al.*, Seasonal investigation of ultrafine-particle organic composition in an eastern Amazonian rainforest, *Atmos. Chem. Phys.*, 2025, **25**, 959–977.
69 A. S. Vishnoi, B. Vansevenant, A. Beji, M. Goriaux, B. Guiot, Y. Azizi, *et al.*, On-board characterization of brake-wear emissions from a Heavy-Duty Vehicle in real-world driving conditions, *Atmos. Environ.: X*, 2025, 100379.
70 X. Hu, Y. Zhao and W. Cheng, Effect of formaldehyde/phenol ratio (F/P) on the properties of phenolic resins and foams synthesized at room temperature, *Polym. Compos.*, 2015, **36**, 1531–1540.
71 P. R. Sarika, P. Nancarrow, A. Khansaheb and T. Ibrahim, Bio-Based Alternatives to Phenol and Formaldehyde for the Production of Resins, *Polymers*, 2020, **12**, 2237.
72 B. Bhatt, U. Marathe, N. Kalel and J. Bijwe, Efficacy of high-performance epoxy resin as a binder to replace eco-unfriendly phenolic resins in Cu-free brake pads, *Tribol. Int.*, 2025, **202**, 110359.
73 M. Křístková, P. Filip, Z. Weiss and R. Peter, Influence of metals on the phenol–formaldehyde resin degradation in friction composites, *Polym. Degrad. Stab.*, 2004, **84**, 49–60.
74 A. B. D. Nandiyanto, M. Fiandini, D. N. A. Husaeni, R. Ragadhita and S. N. Hofifah, Production of Brake Pad from Epoxy Resin: From Polymerization Concept to the Experiment with Analysis of Mechanical Properties, *J. Eng. Res.*, 2022, **25**, 110–115.
75 G. M. Ingo, M. D'Uffizi, G. Falso, G. Bultrini and G. Padeletti, Thermal and microchemical investigation of automotive brake pad wear residues, *Thermochim. Acta*, 2004, **418**, 61–68.
76 M. K. Stanford and V. K. Jain, Friction and wear characteristics of hard coatings, *Wear*, 2001, **251**, 990–996.

77 X. Li, Y. Li, M. J. Lawler, J. Hao, J. N. Smith and J. Jiang, Composition of Ultrafine Particles in Urban Beijing: Measurement Using a Thermal Desorption Chemical Ionization Mass Spectrometer, *Environ. Sci. Technol.*, 2021, **55**, 2859–2868.
78 I. M. Al-Naiema, J. H. Offenberg, C. J. Madler, M. Lewandowski, J. Kettler, T. Fang, *et al.*, Secondary organic aerosols from aromatic hydrocarbons and their contribution to fine particulate matter in Atlanta, Georgia, *Atmos. Environ.*, 2020, **223**, 117227.
79 T. E. Kleindienst, M. Jaoui, M. Lewandowski, J. H. Offenberg and K. S. Docherty, The formation of SOA and chemical tracer compounds from the photooxidation of naphthalene and its methyl analogs in the presence and absence of nitrogen oxides, *Atmos. Chem. Phys.*, 2012, **12**, 8711–8726.
80 K. Kawamura and I. R. Kaplan, Motor exhaust emissions as a primary source for dicarboxylic acids in Los Angeles ambient air, *Environ. Sci. Technol.*, 1987, **21**, 105–110.
81 P. Q. Fu, K. Kawamura, C. M. Pavuluri, T. Swaminathan and J. Chen, Molecular characterization of urban organic aerosol in tropical India: contributions of primary emissions and secondary photooxidation, *Atmos. Chem. Phys.*, 2010, **10**, 2663–2689.
82 B. R. T. Simoneit, P. M. Medeiros and B. M. Didyk, Combustion Products of Plastics as Indicators for Refuse Burning in the Atmosphere, *Environ. Sci. Technol.*, 2005, **39**, 6961–6970.
83 M. D. Leslie, M. Ridoli, J. G. Murphy and N. Borduas-Dedekind, Isocyanic acid (HNCO) and its fate in the atmosphere: a review, *Environ. Sci.: Processes Impacts*, 2019, **21**, 793–808.
84 S. N. Wren, J. Liggio, Y. Han, K. Hayden, G. Lu, C. M. Mihele, *et al.*, Elucidating real-world vehicle emission factors from mobile measurements over a large metropolitan region: a focus on isocyanic acid, hydrogen cyanide, and black carbon, *Atmos. Chem. Phys.*, 2018, **18**, 16979–17001.
85 J. M. Brady, T. A. Crisp, S. Collier, T. Kuwayama, S. D. Forestieri, V. Perraud, *et al.*, Real-Time Emission Factor Measurements of Isocyanic Acid from Light Duty Gasoline Vehicles, *Environ. Sci. Technol.*, 2014, **48**, 11405–11412.
86 D. R. Hanson, P. H. McMurry, J. Jiang, D. Tanner and L. G. Huey, Ambient Pressure Proton Transfer Mass Spectrometry: Detection of Amines and Ammonia, *Environ. Sci. Technol.*, 2011, **45**, 8881–8888.
87 C. Johannessen, J. Liggio, X. Zhang, A. Saini and T. Harner, Composition and transformation chemistry of tire-wear derived organic chemicals and implications for air pollution, *Atmos. Pollut. Res.*, 2022, **13**, 101533.
88 B. Seiwert, P. Klöckner, S. Wagner and T. Reemtsma, Source-related smart suspect screening in the aqueous environment: search for tire-derived persistent and mobile trace organic contaminants in surface waters, *Anal. Bioanal. Chem.*, 2020, **412**, 4909–4919.
89 Berufsgenossenschaft der chemischen Industrie, *Toxicological Evaluations: Dicyclohexylamine*, Berufsgenossenschaft der chemischen Industrie, 2000.
90 T. Singh, M. K. Rathi, A. Patnaik, R. Chauhan, S. Ali and G. Fekete, Application of waste tire rubber particles in non-asbestos organic brake friction composite materials, *Mater. Res. Express*, 2018, **6**, 035703.
91 K. S. Hopstock, Q. Xie, M. A. Alvarado, V. Moschos, S. Bililign, J. D. Surratt, *et al.*, Molecular Characterization and Photoreactivity of Organic Aerosols Formed from Pyrolysis of Urban Materials during Fires at the Wildland–Urban Interface, *ACS ES&T Air*, 2024, **1**, 1495–1506.
92 A. Henriques, N. Paiva, M. Bastos, J. Martins, L. Carvalho and F. D. Magalhães, Improvement of storage stability and physicochemical properties by addition of benzoguanamine in melamine-formaldehyde resin synthesis, *J. Appl. Polym. Sci.*, 2017, **134**, 45185.
93 B. Öztürk and S. Öztürk, Effects of Resin Type and Fiber Length on the Mechanical and Tribological Properties of Brake Friction Materials, *Tribol. Lett.*, 2011, **42**, 339–350.
94 J. LeBras, The Reinforcement of Rubber by Resins, *Rubber Chem. Technol.*, 1962, **35**, 1308–1341.
95 M. C. Lagel, L. Hai, A. Pizzi, M. C. Basso, L. Delmotte, S. Abdalla, *et al.*, Automotive brake pads made with a bioresin matrix, *Ind. Crops Prod.*, 2016, **85**, 372–381.
96 W. F. Rogge, L. M. Hildemann, M. A. Mazurek, G. R. Cass and B. R. T. Simoneit, Sources of fine organic aerosol. 3. Road dust, tire debris, and organometallic brake lining dust: roads as sources and sinks, *Environ. Sci. Technol.*, 1993, **27**, 1892–1904.
97 C. A. Alves, M. Evtyugina, A. M. P. Vicente, E. D. Vicente, T. V. Nunes, P. M. A. Silva, *et al.*, Chemical profiling of PM_{10} from urban road dust, *Sci. Total Environ.*, 2018, **634**, 41–51.
98 J. Zhang, X. Zhang, L. Wu, T. Wang, J. Zhao, Y. Zhang, *et al.*, Occurrence of benzothiazole and its derivates in tire wear, road dust, and roadside soil, *Chemosphere*, 2018, **201**, 310–317.
99 A. Jahanzab, H. Zhao, R. Lu and H. B. Xie, Atmospheric Oxidation Mechanism of 2-Hydroxy-benzothiazole Initiated by Hydroxyl Radicals, *ACS Earth Space Chem.*, 2025, **9**, 457–466.
100 W. Wang, N. V. Karimova, R. B. Gerber and B. J. Finlayson-Pitts, Experimental and Theoretical Investigation of 2-Methylbenzothiazole Oxidation by OH in Air and the Role of O_2 and NO, *J. Phys. Chem. A*, 2025, **129**, 3289–3299.
101 N. V. Karimova, W. Wang, R. B. Gerber and B. J. Finlayson-Pitts, Experimental and theoretical investigation of benzothiazole oxidation by OH in air and the role of O_2, *Environ. Sci.: Processes Impacts*, 2024, **26**, 2177–2188.
102 H. Hagino, Insight into Combustion-Like Wear Processes Due to Unintended CO_2 and Nucleation-Mode Particle Emissions from Passenger Cars at Mild Brake Temperatures (40 °C) under Realistic Driving Conditions, *ACS ES&T Air*, 2025, **2**, 1055–1068.

103 A. Bennett, D. R. Payne and R. W. Court, Pyrolytic and Elemental Analysis of Decomposition Products from a Phenolic Resin, *Macromol. Symp.*, 2014, **339**, 38–47.
104 Y. Li, U. Pöschl and M. Shiraiwa, Molecular corridors and parameterizations of volatility in the chemical evolution of organic aerosols, *Atmos. Chem. Phys.*, 2016, **16**, 3327–3344.
105 B. N. Murphy, N. M. Donahue, A. L. Robinson and S. N. Pandis, A naming convention for atmospheric organic aerosol, *Atmos. Chem. Phys.*, 2014, **14**, 5825–5839.
106 N. M. Donahue, S. A. Epstein, S. N. Pandis and A. L. Robinson, A two-dimensional volatility basis set: 1. organic-aerosol mixing thermodynamics, *Atmos. Chem. Phys.*, 2011, **11**, 3303–3318.
107 G. Isaacman-VanWertz and B. Aumont, Impact of organic molecular structure on the estimation of atmospherically relevant physicochemical parameters, *Atmos. Chem. Phys.*, 2021, **21**, 6541–6563.
108 X. S. Luo, W. Huang, G. Shen, Y. Pang, M. Tang, W. Li, *et al.*, Source differences in the components and cytotoxicity of $PM_{2.5}$ from automobile exhaust, coal combustion, and biomass burning contributing to urban aerosol toxicity, *Atmos. Chem. Phys.*, 2024, **24**, 1345–1360.
109 S. A. Gheni, M. M. Ali, G. C. Ta, H. J. Harbin and S. A. Awad, Toxicity, Hazards, and Safe Handling of Primary Aromatic Amines, *ACS Chem. Health Saf.*, 2024, **31**, 8–21.
110 Y. Wang, X. Li, H. Yang, Y. Wu, Q. Pu, W. He, *et al.*, A review of tire wear particles: Occurrence, adverse effects, and control strategies, *Ecotoxicol. Environ. Saf.*, 2024, **283**, 116782.
111 K. Arole, M. Velhal, M. Tajedini, P. G. Xavier, E. Bardasz, M. J. Green, *et al.*, Impacts of particles released from vehicles on environment and health, *Tribol. Int.*, 2023, **184**, 108417, available from: **https://www.sciencedirect.com/science/article/pii/S0301679X23002049**.
112 A. Volta, S. Sforzini, C. Camurati, F. Teoldi, S. Maiorana, A. Croce, *et al.*, Ecotoxicological effects of atmospheric particulate produced by braking systems on aquatic and edaphic organisms, *Environ. Int.*, 2020, **137**, 105564, available from: **https://www.sciencedirect.com/science/article/pii/S0160412019343521**.
113 Y. Liu, S. Wu, H. Chen, M. Federici, G. Perricone, Y. Li, *et al.*, Brake wear induced PM_{10} emissions during the world harmonised light-duty vehicle test procedure-brake cycle, *J. Cleaner Prod.*, 2022, **361**, 132278.
114 J. N. Smith and A. E. Thomas, Supporting data for: Organic composition of ultrafine particles formed from automotive braking, 2025, DOI: **10.5061/dryad.tmpg4f5bm**.